Catalysis Today 180 (2012) 59–67

Contents lists available at SciVerse ScienceDirect

Catalysis Today

journal homepage: www.elsevier.com/locate/cattod

Shape-dependent catalytic activity of palladium nanoparticles embedded in SiO_2 and TiO_2

Yolanda Pérez[a], M. Luisa Ruiz-González[b], Jose M. González-Calbet[b], Patricia Concepción[c], Mercedes Boronat[c], Avelino Corma[c,*]

[a] Departamento de Química Inorgánica y Analítica, ESCET, Universidad Rey Juan Carlos, 28933 Móstoles, Madrid, Spain
[b] Departamento de Química Inorgánica, Facultad de Químicas, Universidad Complutense, 28040 Madrid, Spain
[c] Instituto de Tecnología Química CSIC-UPV, Universidad Politécnica de Valencia, 46022 Valencia, Spain

ARTICLE INFO

Article history:
Received 15 April 2011
Received in revised form 11 July 2011
Accepted 11 September 2011
Available online 6 October 2011

Keywords:
Palladium nanoparticles
Different shapes
Embedded
Oxidation
Solvent-free
IR spectroscopy of CO adsorption

ABSTRACT

Catalytic studies have shown that the activity of metal nanoparticles depends on their size and shape. Palladium nanoparticles with different morphologies have been prepared and embedded in a SiO_2 and TiO_2 matrix, and their catalytic performance in the solvent-free aerobic oxidation of 1-phenylethanol has been studied. The observed activity is strongly related to the exposed surface sites, being some of the active sites embedded in the matrix or blocked by residual organic species. (1 1 1)/(1 0 0) edge sites are involved in the oxidative dehydrogenation of 1-phenylethanol. The amount of these sites depends on particle morphology. Under our conditions, Pd_{bars}–SiO_2 (Pd nanobars embedded in SiO_2) were found to be the most active.

1. Introduction

The aerobic oxidation of alcohols to ketones and aldehydes is of great interest to obtain a diverse range of intermediates for the synthesis of pharmaceutical and fine chemicals [1]. Catalytic methods are being investigated to perform this reaction under solventless conditions and using molecular oxygen at atmospheric pressure. This represents a much cheaper, safer and more environmentally benign oxidation protocol. Our group has reported the use of Au/CeO_2 (gold nanoparticles supported on cerium oxide) as a highly active catalyst for the selective oxidation of alcohols using oxygen at atmospheric pressure as oxidant in the absence of solvent and base [2]. Palladium supported catalysts have also been reported as Pd/HAP (hydroxyapatite-supported Pd nanoclusters) [3] which shows high TOFs for the oxidation of alcohols under solventless conditions. Recently, Lee and co-workers [4] have presented a Pd/Al_2O_3 (mesoporous alumina-supported palladium) catalyst with high activity for selective aerobic oxidation of allylic alcohols using toluene as solvent but working at lower temperature. Hutchings and co-workers [5] have reported that TiO_2-supported Au–Pd alloy nanocrystals show significantly enhanced activity for alcohol oxidation using green chemistry.

The catalytic activity of nanoparticles is affected by size [6] since the relative ratio of surface atom types (vertex, edge, facets atoms) changes dramatically with varying particle size. In many cases, the activity increases as the particle size decreases due to favourable changes in the electronic properties of surface atoms, which are located mainly on edges and corners in small particles. Kaneda and co-workers [3a] compared two hydroxyapatite-supported Pd nanoclusters with different diameters (3.8 and 7.8 nm) for the oxidation of alcohols and observed higher activities for the catalyst with the smaller particle size. In addition, Wang and co-workers [7] showed that the intrinsic TOF for the oxidation of benzyl alcohol depends on the size of Pd nanoparticles, showing a volcano type curve with a maximum TOF value at a medium size of the Pd nanoparticles (3.6–4.3 nm). Nevertheless, for the oxidation of geraniol or 2-octanol over Pd/NaX it has been demonstrated that the intrinsic TOF does not vary with the size of Pd nanoparticles [8].

On the other hand, the reactivity and selectivity of metal nanocatalysts also depends strongly on the different crystallographic planes present on the nanoparticles and which can be achieved by controlling the morphology of these nanoparticles [9]. Klabunde and co-workers [10] concluded that MgO hexagonal crystals containing {1 0 0} planes are more active for the

* Corresponding author.
E-mail address: acorma@itq.upv.es (A. Corma).

0920-5861/$ – see front matter © 2011 Elsevier B.V. All rights reserved.
doi:10.1016/j.cattod.2011.09.011

benzylation of toluene than polycrystalline and nanocrystalline samples. Li and co-workers [11] demonstrated that CeO_2 nanorods with well-defined planes {0 0 1} and {1 1 0} show higher CO oxidation activity than CeO_2 nanoparticles with {1 1 1} facets because of their more reactive planes. El-Sayed and co-workers [9a] showed that the tetrahedral Pt nanoparticles are the most catalytically active in electron-transfer reactions, while the cubic nanoparticles are the least catalytically active. They [12] also studied the effect of the tetrahedral and cubic shape on the stability of Pt nanoparticles colloids used in the Suzuki reaction. For this reaction they observed that the tetrahedral and cubic shape changes during the course of the reaction causing a rapid decrease in the catalytic activity. There are very few studies in which nanoparticles with defined morphologies are deposited onto supports [13]. However, this could prevent nanoparticle shape changes while providing the inherent advantages of a heterogeneous catalyst, such as easy recovery and separation.

Various methods have been reported for producing Pd nanoparticles with different shapes. Xia and co-workers [14] have prepared a variety of Pd nanocrystals as cubes, cuboctahedra, and nanoplates by manipulating the reduction kinetics of the polyol method, using ethylene glycol (EG) in the presence of poly(vinylpyrrolidone) (PVP) with addition of Fe(III) species. More recently [15], they have achieved Pd nanobars, nanorods and icosahedra without the presence of Fe(III) demonstrating that PVP is a capping agent and also a good reductant. Rafailovich and co-workers [16] have synthesized rectangular Pd nanoparticles in the presence of a surfactant, cetyltrimethylammonium bromide and with trisodium citrate using ascorbic acid as reductant agent. Instead, Hyeon and co-workers [17] have used triblock Pluronic copolymers as capping agents for the synthesis of Pd nanoparticles of various shapes.

The purpose of our present work is to study the catalytic activity and stability of palladium nanoparticles with different shapes. In order to do that, SiO_2-embedded and TiO_2-embedded Pd nanoparticles with different morphologies such as bars, rods and icosahedra were prepared and characterised using transmission electron microscopy (TEM), high-resolution transmission electron microscopy (HRTEM), X-ray diffraction (XRD), thermogravimetric analysis, inductively coupled plasma (ICP), N_2 adsorption–desorption, hydrogen chemisorptions and IR spectroscopy of CO. In order to evaluate the dependency of catalytic performance on particle shape, the catalysts were tested in the oxidation of 1-phenylethanol under solventless conditions and using molecular oxygen at atmospheric pressure. In addition, we have examined the stability of the catalysts using HRTEM characterisation before and after catalysis.

2. Experimental

2.1. Materials

Acetone, ethanol (Scharlau, analytical grade, 99.5%), and milliQ water (MILLIPORE) were used as solvents. Sodium palladium(II) tetrachloride (Na_2PdCl_4, 99.995% trace metals basis), 1-phenylethanol (98%), ethylene glycol (EG, ≥99%), poly(vinylpyrrolidone) (PVP, MW = 55,000), citric acid (≥99.5%) potassium bromide (KBr, 99.99% trace metals basis), sodium hydroxide (NaOH, ≥98%), ammonium fluoride (NH_4F, ≥98.0%), hydrogen peroxide solution (30 wt% in H_2O) and sulfuric acid (H_2SO_4, 95.0–98.0%) were purchased from Sigma–Aldrich and used as received. Tetraethyl orthosilicate (TEOS, Aldrich, ≥99.0%) and titanium tetrabutoxide ($Ti(OBu_n)_4$), Fluka, ≥97.0%) were employed to prepare SiO_2 and TiO_2, respectively.

2.2. Catalysts preparation

2.2.1. Synthesis of palladium nanobars (Pd_{bars})

Palladium nanobars were prepared with similar procedure of Xia and co-workers [15a]. A 100-mL two-necked round bottomed flask, equipped with a condenser and magnetic stirrer, was charged with 20 mL of EG and heated at 100 °C under stirring. Meanwhile, two solutions were prepared, PVP (0.366 g, 3.29 mmol) in 12 mL of water and $Na_2[PdCl_4]$ (0.194 g, 0.66 mmol) and KBr (2.4 g, 20.2 mmol) in 12 mL of water. Both solutions were injected simultaneously into the flask at a rate of 45 mL h^{-1} using a two-channel syringe pump. The mixture was stirred at 100 °C for 1 h to afford a red colloidal Pd solution.

2.2.2. Synthesis of palladium nanorods (Pd_{rods})

Palladium nanorods were prepared using a procedure similar to that described in Section 2.2.1, except that in this case the PVP was dissolved in 12 mL of EG.

2.2.3. Synthesis of palladium icosahedra (Pd_{icos})

Palladium icosahedra were prepared with a procedure similar to that reported by Xia and co-workers [15b]. A 100-mL two-necked round bottomed flask, equipped with a condenser and magnetic stirrer, was charged with a solution of PVP (0.142 g, 1.28 mmol) and citric acid (0.24 g, 1.25 mmol) in water (32 mL) and heated in an oil bath at 90 °C under stirring. To this solution was added by syringe, $Na_2[PdCl_4]$ (0.075 g, 0.25 mmol) in water (12 mL). The mixture was stirred at 90 °C for 26 h to obtain a brown colloidal Pd solution.

2.2.4. Synthesis of SiO_2-embedded palladium nanoparticles

The preparation of the SiO_2-embedded Pd nanoparticles was based on the sol–gel process [18] in the presence of PVP-capped npPd. The procedure consisted in adding 30 mL of ethanol and 7.4 mL of tetraethyl orthosilicate (TEOS) to 22 mL of the aqueous solution containing the capped npPd. The hydrolysis was catalysed by 2.4 mL of a 0.0434 M aqueous solution of NH_4F. The sol, under continuous stirring and heating at 50 °C became a gel that in 24 h converted to a powder. The powder was dried overnight at 60 °C.

2.2.5. Synthesis of TiO_2-embedded palladium nanoparticles

The preparation of the TiO_2-embedded Pd nanoparticles was also based on the sol–gel process [18] in the presence of PVP-capped npPd. In this case, the procedure consisted in adding 23.4 mL of ethanol and 9.6 mL of titanium tetrabutoxide ($Ti(OBu_n)_4$) to 22 mL of the aqueous solution containing the capped npPd. The hydrolysis was catalysed by 7.2 mL of a 0.0434 M aqueous solution of NH_4F. The sol, under continuous stirring and heating at 50 °C became a gel that in 24 h converted to a powder. The powder was dried overnight at 60 °C.

2.2.6. Removal of the capping ligands from SiO_2 or TiO_2-embedded palladium nanoparticles

The extraction of the capping ligands was carried out by two treatments. In a first step, 1 g of SiO_2 or TiO_2-embedded palladium nanoparticles was treated with 40 g of 30% H_2O_2 solution and heated for 16 h at 95 °C. The solid was filtered and washed with water and ethanol. Then, the solid was dried at 60 °C overnight. For the second treatment, 1 g of the resulting solid was mixed with 60 g of 0.1 M H_2SO_4 solution and heated for 24 h at 70 °C. The solid was filtered and washed with water and ethanol. Finally, the solid was dried at 60 °C overnight.

2.3. Catalysts characterisation

Crystallinity and phase identification of the materials were determined by powder X-ray diffraction (XRD) in a Philips X'Pert

MPD diffractometer equipped with a PW3050 goniometer (Cu Kα radiation, graphite monochromator), provided with a variable divergence slit. The metal content of the samples was determined by using an inductively coupled plasma emission spectrophotometer Varian 715-ES. Surface area and pore volume of the samples were measured by nitrogen adsorption experiments at 77 K, using a Micromeritics ASAP 2000 apparatus. Thermogravimetric and differential thermal analyses (TGA–DTA) were performed in a Netzsch STA 409 EP thermal analyzer with about 20 mg of sample and a heating rate of 10 °C min^{-1} in air flow (6 L h^{-1}). Hydrogen chemisorptions were recorded by Micromeritics ASAP 2020 Chemi. Transmission electron microscope (TEM) micrographs of colloids nanoparticles were collected in a Philips CM-10 microscope operating at 100 kV. High-resolution transmission electron microscopy (HRTEM) were recorded by JEOL JEM-3000F microscope equipped with an Oxford Instruments ISIS 300 X-ray microanalysis system and a LINK "Pentafet" detector for EDS analyses. FTIR spectra were collected with a "Nexus" Thermo spectrometer equipped with a DTGS detector. An IR cell allowing in situ treatments in controlled atmospheres and temperatures has been connected to a vacuum system with gas dosing facility. The samples (∼6 mg) were pretreated in an H_2 (10%) flow at 80 °C for 1 h, followed by vacuum treatment (10^{-5} mbar) at 200 °C 1 h. It has been observed that this treatment does not modify the amount of residual organic species on the sample, their only effect is to reduce Pd species which has been oxidized by contact with air. CO adsorption experiments were performed at 25 °C at different CO dosing (1–20 mbar).

2.4. General procedure for the solvent-free aerobic oxidation of 1-phenylethanol

1-Phenylethanol (0.6 mL, 5 mmol) was added over catalyst (0.12 mol%) in a 10-mL two-necked round bottomed flask, equipped with a condenser and magnetic stirrer and molecular oxygen (1 atm) was bubbled continuously through the suspension. The mixture was heated at 110 °C. After the reaction, acetone was injected into the flask and the catalyst was separated by centrifugation. The products in the solution were analyzed by GC–MS and conversion and selectivity were determined by GC. The catalyst was recovered by filtration, washed with 1 M NaOH solution and dried in vacuum.

3. Results and discussion

Palladium nanorods (Pd_{rods}) and nanobars (Pd_{bars}) were prepared via reduction of $Na_2[PdCl_4]$ by EG and PVP and in the presence of KBr. The terminal hydroxyl groups of PVP serve as a mild reducing agent and stabilizer for the formation of metal nanoparticles [19]. In addition, the introduction of bromide into the reaction promoted the formation of different facets since the bromide is able to chemisorb onto the surface of Pd and alter the order of surface free energies for different facets [15a]. The low magnification TEM image (Fig. 1a) shows the occurrence of highly dispersed Pd_{bars} with width between 4 and 6 nm. Fig. 1b shows low magnification TEM image of Pd_{rods} with diameters between 4 and 6 nm. Pd nanoparticles with icosahedral shape (Pd_{icos}) were synthesized by reduction of $Na_2[PdCl_4]$ by citric acid using PVP as stabilizer to avoid aggregation and to direct the growth the nanoparticles into icosahedral form [15b]. Fig. 1c shows the low magnification TEM image of Pd_{icos} with diameters between 7 and 12 nm.

In this work, PVP-capped Pd nanoparticles were embedded in a silica or titania matrix by sol–gel method. However, the SiO_2 or TiO_2-embedded palladium nanoparticles thus prepared are capped by PVP and do not posses catalytic properties. It is clear that the accessible surface area strongly increases by removing the organic components. Therefore, to obtain a material which presents high catalytic activity it is necessary to remove the organic species from the as-made material. The most common method consists of calcining the materials in an air or oxygen flow, but during calcination the nanoparticle shape may change dramatically. Alternative methods to extract organic templates have been reported such as liquid extraction using acidic solutions, neutral salt solutions, alcohols, or mixtures of these [20]. Other mild procedures have been used as

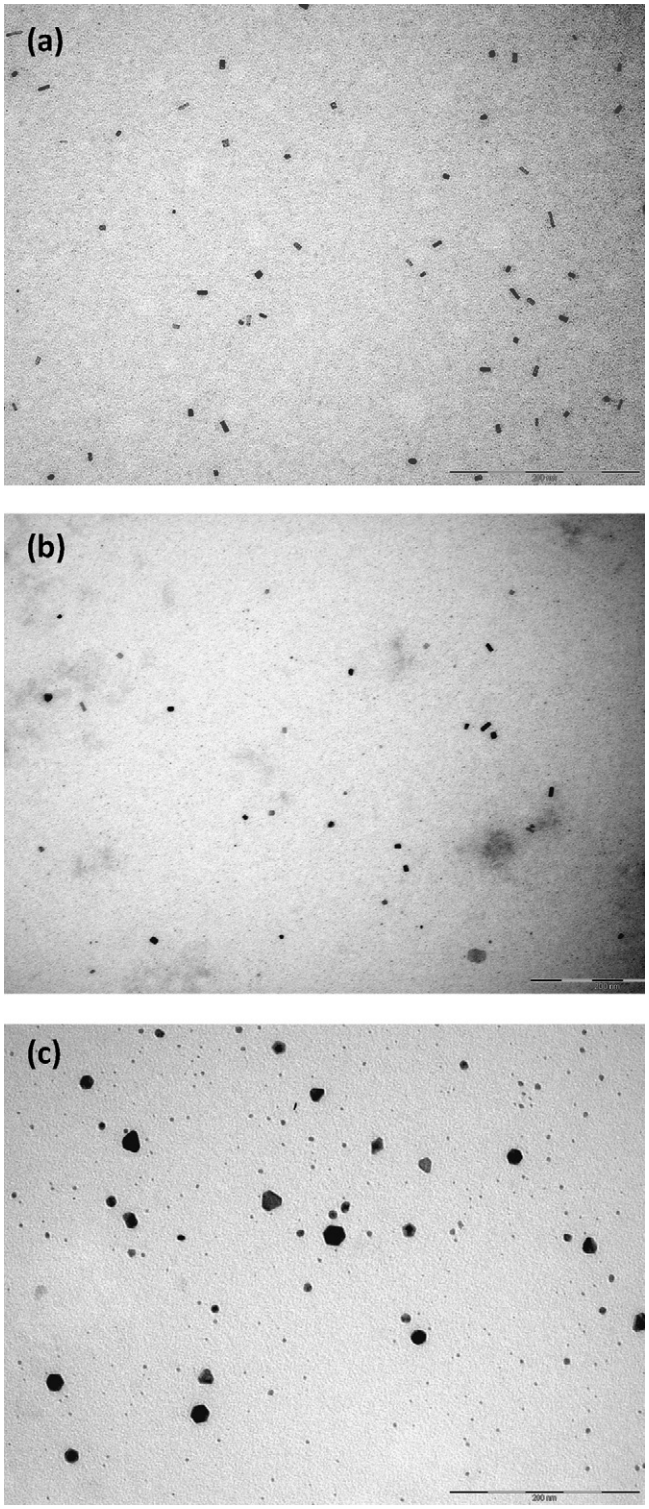

Fig. 1. TEM images of the PVP-capped palladium nanoparticles synthesized with different shape (a) bars, (b) rods and (c) icosahedral.

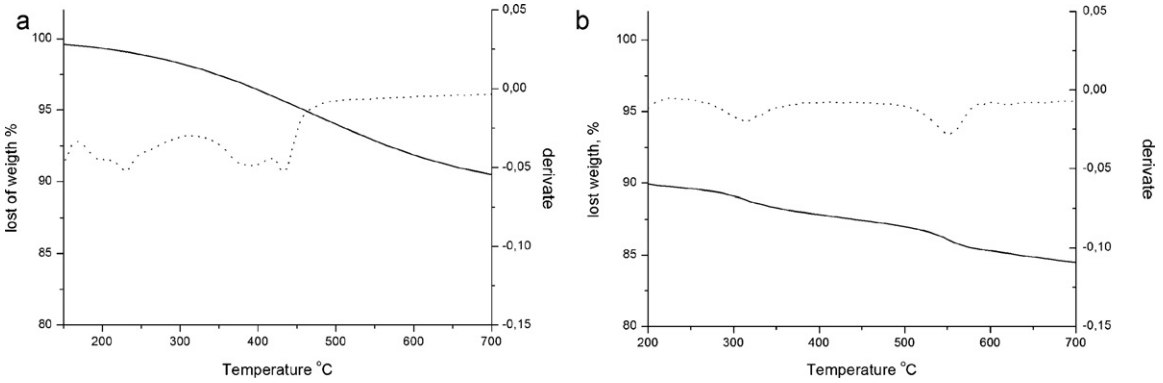

Fig. 2. Thermogravimetric profile of the (a) Pd_{icos}–SiO_2 material (without removing the organic ligands) and (b) final Pd_{icos}–SiO_2 material.

the treatment of SBA-15 in presence of nitric acid and H_2O_2 [21]. In this work, a procedure based on two steps was chosen to remove organic components. In the first treatment, SiO_2 or TiO_2-embedded palladium nanoparticles were suspended in 30% aqueous solution of H_2O_2 for 16 h at 95 °C and, in the second step, the resulting solid was treated with 0.1 M solution of H_2SO_4. The final materials were washed with water and ethanol and dried in an oven at 60 °C overnight. The thermal decomposition of the organic ligands of sample Pd_{icos}–SiO_2 (without removing the organic ligands) can be observed in the thermogravimetric profile shown in Fig. 2a. After treatment with the aqueous solution of H_2O_2 and with aqueous solution of H_2SO_4 some organic material still remains adsorbed on the Pd_{icos}–SiO_2 material (Fig. 2b), being the washing process under mild conditions not complete.

Table 1 summarises the textural characteristics, content and dispersion of palladium in SiO_2 and TiO_2-embedded palladium nanoparticles. The quantity of loaded palladium was determined by ICP measurement. The BET surface area and average pore diameter of the different materials were determined from the corresponding N_2 adsorption–desorption isotherms. The Pd–SiO_2 materials showed higher BET surface area than the Pd–TiO_2 materials. Nevertheless, the BJH calculations showed average pore diameters smaller for the Pd–SiO_2 materials. Hydrogen chemisorption over the Pd materials shows similar values in all samples giving a dispersion value between 11 and 17%. But care should be taken with the values obtained by H_2 chemisorption since hydrogen diffusion into the bulk of the metal can occur, and our metal dispersion results could be overestimated. For this reason, a more detailed study based on CO adsorption followed by IR spectroscopy has been done.

The X-ray diffraction (XRD) patterns of Pd_{bars} and Pd_{rods} embedded in SiO_2 or TiO_2 do not exhibit any detectable reflection from Pd, indicating that the Pd nanoparticles are too small to be detected by XRD. In contrast, the XRD pattern of Pd_{icos}–SiO_2 (Fig. 3), shows broad reflexion related to silica and characteristic reflections (1 1 1), (2 0 0) and (2 2 0) of Pd (face-centred-cubic).

Table 1
Textural characteristics of the materials, content and dispersion of palladium in SiO_2 and TiO_2-embedded palladium nanoparticles.

Catalyst	Pd (wt%)	Pd dispersion[a] (%)	BET surface area [$m^2\ g^{-1}$]	Average pore diameter [Å]
Pd_{bars}–SiO_2	1.5	11.5	597	28.29
Pd_{bars}–TiO_2	1.3	12.3	297	65.21
Pd_{rods}–SiO_2	1.6	14.4	475	28.19
Pd_{rods}–TiO_2	1.5	17.8	307	40.21
Pd_{icos}–SiO_2	1.4	14.1	750	23.61
Pd_{icos}–TiO_2	1.5	15.5	210	66.02

[a] Calculated from H_2 chemisorption.

The palladium nanoparticles embedded in SiO_2 show differences, especially concerned to their shape and distribution, with respect to the original non supported ones. First of all, the highly dispersed arrangement is, in the three cases, substituted by a bit of aggregation one, as seen in Fig. 4 . On the other hand, the embedded particles lost the dominant morphology exhibited in solution becoming some of them rounder, which is due to the melting of the Pd particles during the removal of organic materials [22]. Actually, three types, polyhedral, bars and rods, coexist on the supported samples originally labelled as for Pd_{icos}, Pd_{bars} and Pd_{rods}. Moreover, in addition to the above patterns less abrupt polyhedral particles as well as spherical ones also appear. Indeed, this new shape is predominant on the Pd_{icos} and Pd_{bars} samples, as observed in Fig. 4a and b, respectively, whereas a more dispersed situation is found for Pd_{rods}, as seen in Fig. 4c. This observation allows to conclude that the anisotropic forms tend to be more isotropic, in accordance with thermodynamics [15a].

Actually, particle morphology is related to the crystallographic surfaces that enclose them, i.e., to the relative crystallographic orientation. This structural information is provided by means of HRTEM. This study shows that the fcc Pd particles exhibiting polyhedral and spherical morphologies are mainly orientated along [0 1 $\bar{1}$] zone axis while elongated particles, named as bars, are orientated along [0 1 0]. Fig. 5 is a HRTEM image corresponding to Pd_{icos} sample showing a characteristic polyhedral particle. The measured interlayer periodicities (A) and the corresponding Fast Fourier Transform (FFT) (A_{FFT}) are characteristic of Pd fcc along [0 1 $\bar{1}$] zone. Moreover, notice that the particle is twinned, as clearly shown in the FFT (B_{FFT}) performed on an area including two domains (marked

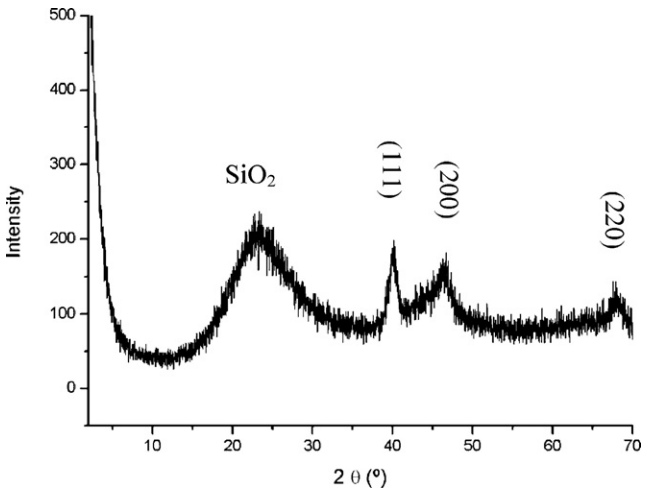

Fig. 3. XRD pattern of Pd_{icos}–SiO_2 material.

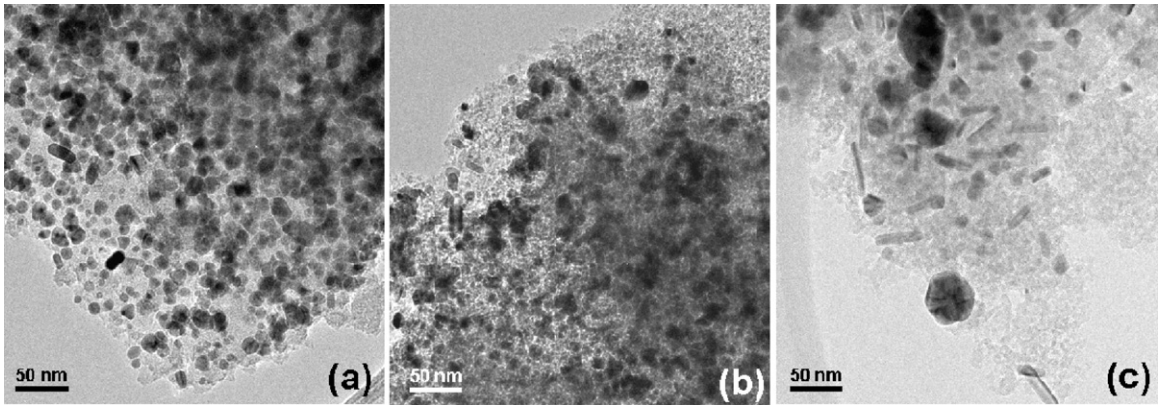

Fig. 4. Low magnification images corresponding to SiO_2 embedded particles (a) Pd_{icos}, (b) Pd_{bars} and (c) Pd_{rods} before catalysis.

in image). Fig. 6 is an image of a more striking polyhedral particle exhibiting multitwining. In fact, twining is a quite frequent defect appearing in fcc metallic nanoparticles at small sizes [23]. Fig. 7 is a HRTEM image corresponding to a Pd_{bars} sample showing two particles, one of them elongated and another one spherical. The orientation of the spherical one (A) is again along [0 1 $\bar{1}$] zone, whereas for the elongated one distances (B) and the corresponding FFT (B_{FFT}) evidence a different orientation in agreement to the [0 1 0] zone axis.

Since the Pd nanoparticles are embedded in a SiO_2 or a TiO_2 matrix, and according to BET analysis the average pore diameter is relative low in the case of SiO_2 as compared to TiO_2, we can assume that not all the Pd atoms are exposed to the reactants, remaining a high fraction of Pd sites encapsulated by the support. Moreover, the presence of remaining PVP molecules, not completely eliminated by the washing procedure, could also block a number of active surface sites. Thus, the presence of the SiO_2 and TiO_2 matrix and PVP molecules could alter the nature and proportion of exposed defect sites versus facetted sites of the studied Pd samples, independent of the morphology of the samples obtained by HRTEM. In order to gain a deeper insight into the nature of exposed active sites IR spectroscopy of CO adsorption has been performed. CO has been reported as a very sensitive probe molecule for metal characterisation [24].

IR spectra of CO adsorption at 25 °C on the Pd samples are shown in Fig. 8. As can be observed, the exposed surface sites are not directly related to their particle morphology. Thus, an encapsulation effect due to the support matrix and/or the presence of remaining organic molecules (PVP) can be inferred. On both Pd samples with an initial nanobar morphology embedded in SiO_2 and TiO_2, an IR band at 2057 cm^{-1} is observed. In addition to this band, on the Pd_{bars}–TiO_2 sample other bands at 2085, 1975 and 1919 cm^{-1} are observed. The IR bands at 2085 cm^{-1} can be ascribed to CO linearly bonded to a (1 1 1) facet, while the IR band at 2057 cm^{-1} can be ascribed to CO linearly bonded to (1 1 1)/(1 0 0) particle edges [25], and the 1975 and 1919 cm^{-1} IR bands correspond to bridge CO species on (1 0 0) planes and defect sites [25]. A similar IR band at 2057 cm^{-1} but less intense than in the other two

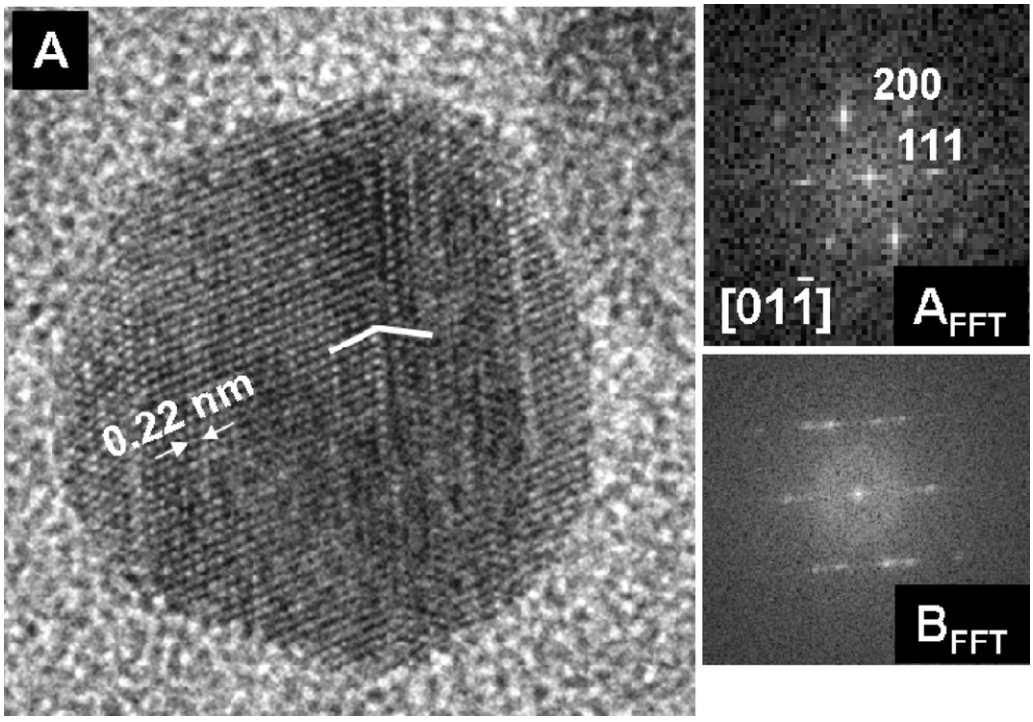

Fig. 5. High resolution image corresponding to Pd_{icos}–SiO_2 material (A) and corresponding FFT's of twinned domains (A_{FFT} and B_{FFT}).

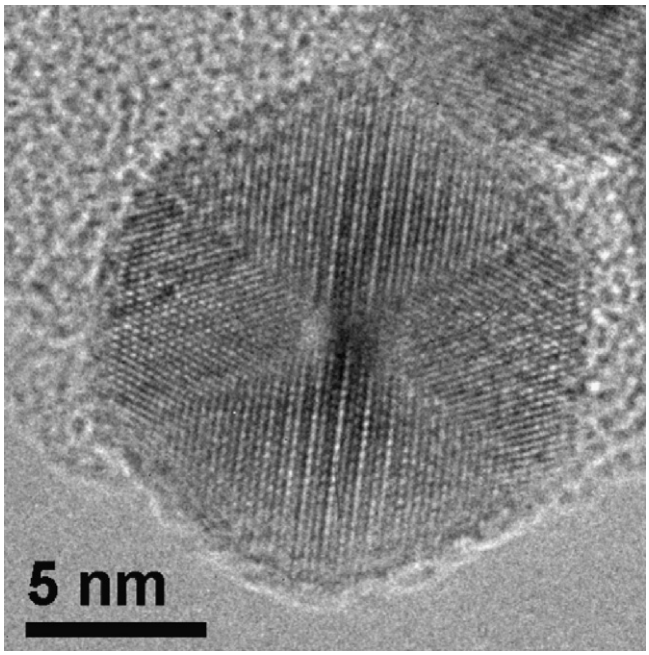

Fig. 6. Multitwinned particle characteristic of Pd_{icos}–SiO_2 sample.

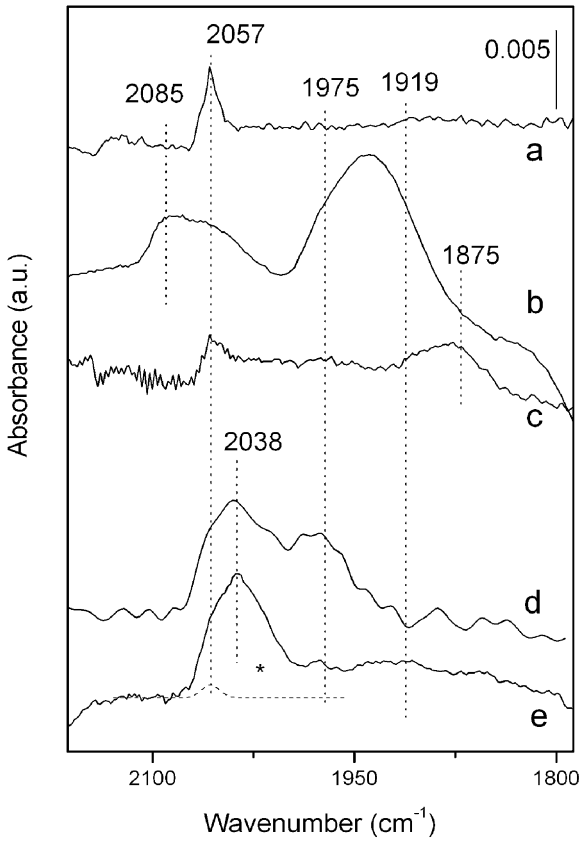

Fig. 8. FTIR spectra of CO adsorption (20 mbar) at 25 °C on (a) Pd_{bars}–SiO_2, (b) Pd_{bars}–TiO_2, (c) Pd_{icos}–SiO_2, (d) Pd_{icos}–TiO_2, (e) Pd_{rods}–TiO_2 samples. (*) peak of decovolution.

samples, is observed in the Pd sample with icosahedra morphology embedded in a SiO_2 matrix. Very low intense IR bands at 1975 and 1875 cm^{-1} associated to bridge CO species and CO adsorbed on hollow sites of Pd(1 1 1) planes are also observed. However, when the same Pd sample with icosahedra morphology is embedded in a TiO_2 matrix, Pd_{icos}–TiO_2 sample, a completely different spectra is obtained. In this case an IR band at lower frequencies, 2038 cm^{-1}, predominate, which can be ascribed to CO bonded to highly defective sites, such as low coordinated Pd atoms [26], or due to CO in a tilt configuration interacting simultaneously with Pd and Ti^{4+} Lewis sites [27]. A similar low frequency IR band at 2038 cm^{-1} is mainly observed in the Pd sample with nanorod morphology embedded in a TiO_2 matrix, Pd_{rods}–TiO_2 sample. On both Pd_{icos}–TiO_2 and Pd_{rods}–TiO_2 samples, broad and very low intense IR bands at 1975 and 1919 cm^{-1} are also observed associated to CO bridge species on (1 0 0) planes or defects, together with a very small contribution of the IR band at 2057 cm^{-1}. The low intensity of the last IR band could be due to the encapsulation effect of the TiO_2 matrix or to the remaining organic species that block the accessibility of extended surface facets toward reactive molecules.

Indeed, pre-treatment of the Pd_{rods}–TiO_2 sample at 150 °C in a 10% H_2 flow leads to a substantial release of the remaining organic molecules (IR bands at 1675, 1615, 1534, 1435, 1321 and 1256 cm^{-1}, see Fig. 9), and to the appearance of high extended surface sites (IR bands at 2120, 2100 cm^{-1} (CO linearly bonded to (1 1 1) terraces) and 2057 cm^{-1} (CO linearly bonded to (1 1 1)/(1 0 0) edges)), in addition to the previously observed IR bands at 2038 and 1975 cm^{-1} (Fig. 9). However, in the Pd_{icos}–TiO_2 sample, even after

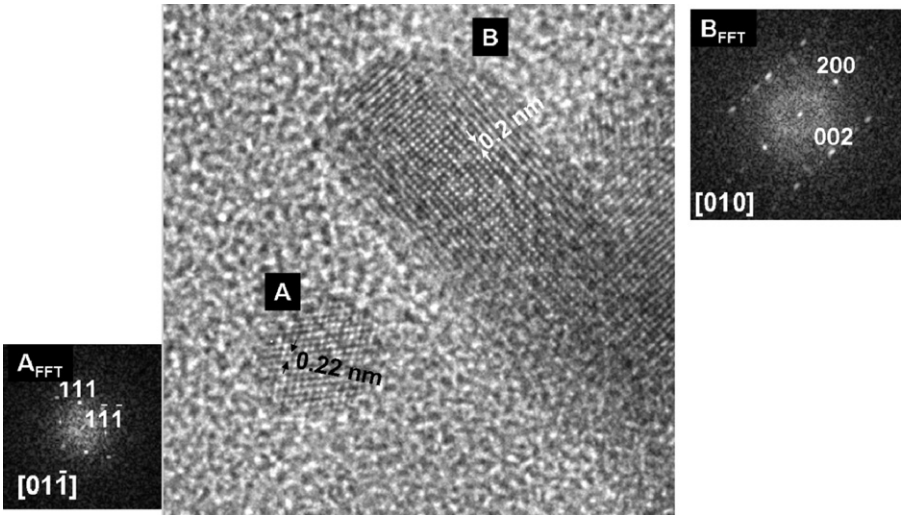

Fig. 7. High resolution image corresponding to embedded Pd_{bars}–SiO_2 showing two kind of particles (A and B) and the corresponding FFT (A_{FFT} and B_{FFT}).

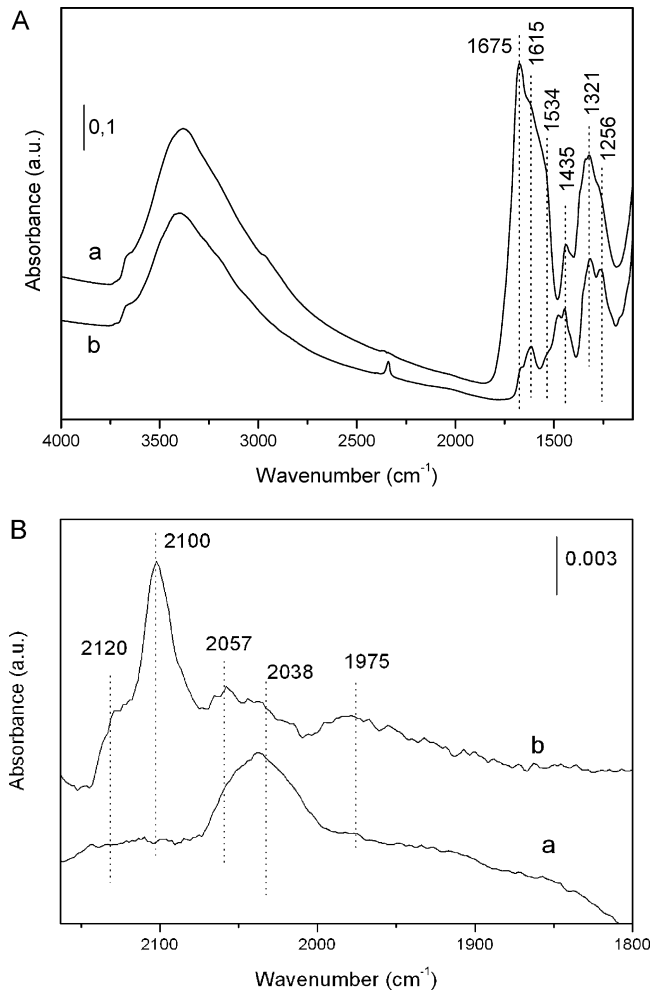

Fig. 9. (A) FTIR spectra of the Pd_{rod}–TiO_2 sample reduced at (a) 80 °C 10%H_2, (b) 150 °C 10%H_2. (B) FTIR spectra of CO adsorption (20 mbar) at 25 °C on the Pd_{rod}–TiO_2 sample reduced at (a) 80 °C 10%H_2, (b) 150 °C 10%H_2.

further elimination of the organic species at 150 °C in 10% H_2 flow the IR spectra remain the same, due to the encapsulation effect of the TiO_2 matrix. In a similar way, in the Pd_{icos}–SiO_2 sample the amount of remaining organic species observed from their IR spectra is quite low, however the amount of surface sites detectable by CO adsorption is very low (low infrared intensity), which should be related to the encapsulation effect of the SiO_2 matrix with a small pore diameter (2.8 nm).

In conclusion, the presence of adsorbed organic species and of the embedding inorganic matrix has a strong influence on the number and type of exposed catalytic active sites, something that has to be taken into consideration when trying to explain their catalytic performance.

The obtained Pd nanoparticles embedded in SiO_2 and TiO_2 were used as catalysts for the oxidation of 1-phenylethanol. The reactions were carried out at 110 °C, atmospheric pressure by bubbling oxygen and without solvent. The results obtained with the six different synthesized catalysts and Pd/HA (palladium nanoparticles supported on hydroxyapatite) [28] are given in Table 2. Different catalytic activity for oxidation of 1-phenylethanol was observed in the different materials, affording in all cases the corresponding carbonyl compound, acetophenone, with excellent selectivity 100%.

The catalysts with SiO_2 as support give significant higher reaction rates, compared to the counterpart catalysts with TiO_2 as support. Of all six catalysts, Pd_{bars}–SiO_2 presents the highest

Table 2
Aerobic oxidation of 1-phenylethanol catalysed by the different materials.[a]

Catalyst	Conversion (%)		
	10 min	30 min	2 h
Pd_{bars}–SiO_2	66	93	98
Pd_{bars}–TiO_2	33	56	90
Pd_{rods}–SiO_2	10	28	86
Pd_{rods}–SiO_2 (calcined)[b]	–	15	50
Pd_{rods}–TiO_2	2	6	59
Pd_{icos}–SiO_2	14	33	84
Pd_{icos}–TiO_2	3	23	73
Pd/HA[c]	53	85	99

[a] Reaction conditions: 1-phenylethanol (5 mmol), Pd catalyst (Pd: 6 μmol), 110 °C, 1 atm of O_2.
[b] Pd_{rods}–SiO_2 calcined in air at 450 °C.
[c] Prepared by impregnation of HAP with $PdCl_2(PhCN)_2$ [Ref. 28].

activity for the oxidation of 1-phenylethanol, even higher than Pd/HA (see Fig. 10). Pd_{bars}–SiO_2 catalyst exhibits an excellent selectivity to acetophenone (100%) and rapid conversion (66%, in 10 min and 93% in 30 min), higher than that reported by Suzuki and co-workers [29] for Pd/CeO_2/O-Dia catalyst (77.8% conversion at 100 °C for 4 h and using *o*-xylene as solvent) and those reported for Pd/NaX (palladium nanoparticles over NaX zeolite) (TOF (based on the total Pd atoms) = 627 h^{-1} [8] compared to a value of 3313 h^{-1} achieved on Pd_{bars}–SiO_2 after 10 min, with similar reaction conditions.

Comparing the catalytic behaviour of the Pd samples with the CO-IR spectra it can be observed that samples showing highly defective Pd atoms or defective Pd atoms in close proximity to Ti^{4+} surface sites (IR band at 2038 cm^{-1}) (Pd_{icos}–TiO_2 and Pd_{rods}–TiO_2) present a very low initial activity compared to those samples in which (1 1 1)/(1 0 0) edge sites are present (Pd_{bars}–SiO_2, Pd_{bars}–TiO_2, and Pd_{icos}–TiO_2). On the other hand, comparing the activity of the last three samples with their CO-IR spectra, the (1 1 1) facet seems not to be involved in the catalytic activity, while (1 1 1)/(1 0 0) edges (IR band at 2057 cm^{-1}) seem to be the active surface sites in the oxidation of the alcohol. Mori et al. [3b] attributed defective surface sites as the catalytic active sites involved in the β-hydride elimination, being this rate limiting step of the reaction. According to Ferri et al. [25c] alcohol dehydrogenation to the carbonyl product occurs on all Pd sites, whereas product decomposition occurs predominantly on (1 1 1) planes. Chen et al. [7], however, proposed that an appropriate ratio of defect sites to facet sites is required for the conversion of benzyl alcohol. Our

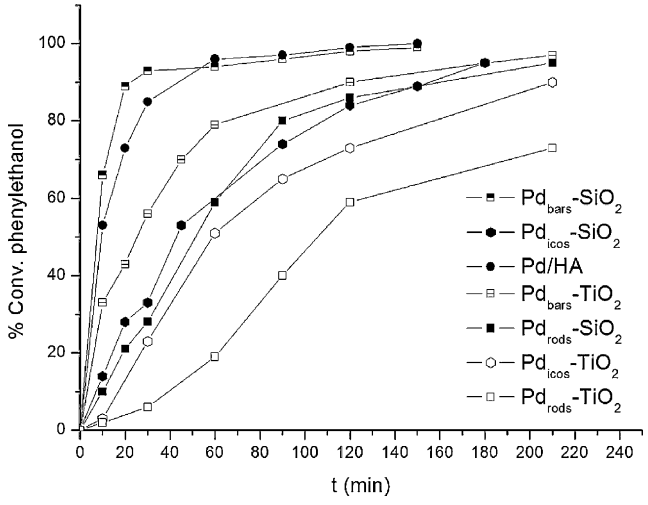

Fig. 10. Conversion of 1-phenylethanol versus reaction time with the different materials.

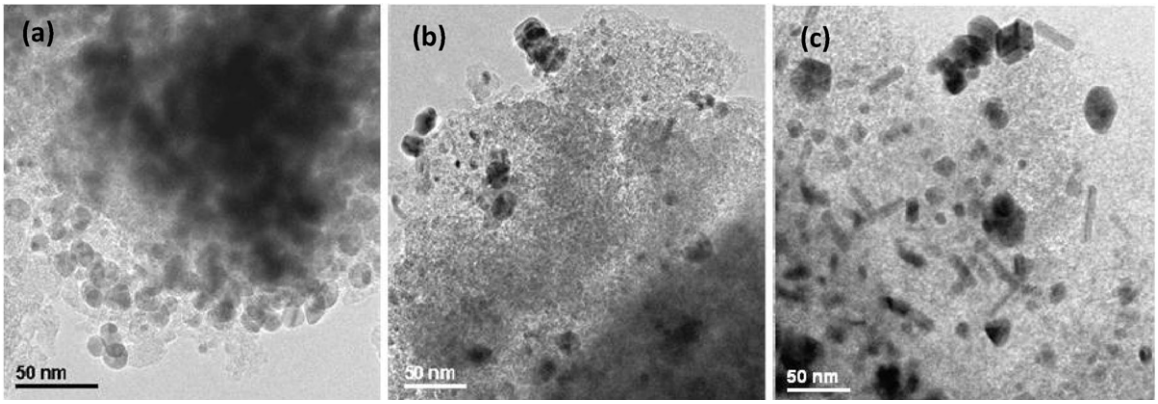

Fig. 11. Low magnification images corresponding to SiO_2 embedded particles (a) Pd_{icos}, (b) Pd_{bars} and (c) Pd_{rods} after catalysis.

results show that (1 1 1)/(1 0 0) edge sites are involved in the dehydrogenation of the alcohol, while adsorption of the aromatic ring on the (1 0 0) face could enhance the interaction of the hydroxyl group with a neighbouring Pd surface site. Highly defective isolated Pd atoms or $Pd–Ti^{4+}$ surface sites are less reactive. Interestingly, an increase in activity with reaction time is observed very clearly in the less reactive samples ($Pd_{icos}–TiO_2$ and $Pd_{rods}–TiO_2$) and not so clearly in the other samples. Removal of organic species under reaction conditions could in part be responsible for the increased activity by leading new accessible active surface sites. However clear evidence by IR spectroscopy cannot be obtained due to the presence of reaction products adsorbed on the surface of the final catalysts, which disables characterisation of the catalysts surface. If removal of organic species takes place, the final activity achieved by all catalysts should be related to the final amount of exposed surface sites, which depends on their crystal morphology determined by HRTEM.

In order to study the stability the possibility to recycle the catalysts, they were recovered by filtration, washed with 1 M NaOH solution and dried in vacuum. After catalysis, the variety of morphologies is kept (Fig. 11) confirming the stability of catalyst. The fcc twinned structure is also maintained as seen in Fig. 12 corresponding to a characteristic HRTEM image of $Pd_{icos}–SiO_2$ after catalysis.

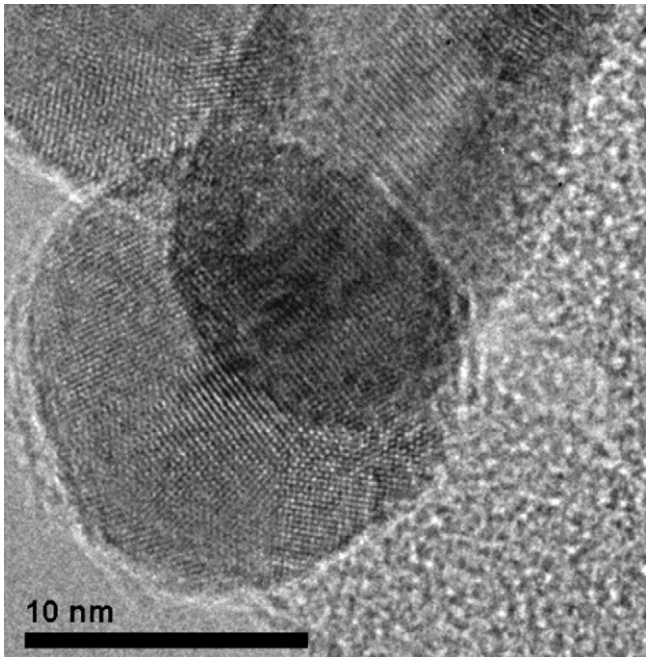

Fig. 12. HRTEM image corresponding to a characteristic $Pd_{icos}–SiO_2$ after catalysis.

Table 3
Recycle of $Pd_{bars}–SiO_2$ for oxidation of 1-phenylethanol.[a]

No. of cycle	1	2	3
Conversion (%)	97	96	93

[a] Reaction conditions: 1-phenylethanol (5 mmol), Pd catalyst (Pd: 6 μmol), 110 °C, 1 atm of O_2.

The recovered $Pd_{bars}–SiO_2$ catalyst was used in 3 consecutive runs without observing important decay in its catalytic activity (Table 3). This reusability also demonstrates the stability of these materials. The Pd content in the recovered catalyst after the first run was measured by ICP obtaining 1.5 wt%, the same value as before the reaction. Even more, the recovered catalyst did not show any Pd leaching.

4. Conclusions

Palladium nanoparticles with different shapes were synthesized and embedded in a SiO_2 and TiO_2 matrix. The catalysts were tested in the oxidation of 1-phenylethanol under solventless conditions and using O_2 at atmospheric pressure. The presence of a SiO_2 and TiO_2 matrix and the presence of remaining organic species have a strong influence on the exposed surface sites, by encapsulating or blocking some sites, independently on the particle morphology determined by HRTEM. Thus, accurate characterisation of surface sites by a surface sensitive tool is strongly recommended, since catalytic activity is related to the exposed surface sites. According to our results (1 1 1)/(1 0 0) edge sites are involved in the oxidative dehydrogenation of 1-phenylethanol. Removal of some organic species under reaction conditions increasing the amount of exposed surface sites and accordingly enhancing catalytic activity could explain the increased activity observed on all samples with time of reaction. Indeed, IR spectroscopy of CO adsorption showed an increase of exposed surface sites on the $Pd_{icos}–TiO_2$ sample after release of organic species. The final amount of exposed active surface sites depends on the particle morphology. Under our conditions, $Pd_{bars}–SiO_2$ catalyst exhibits excellent selectivity to acetophenone (100%) and rapid conversion (66%, in 10 min and 93% in 30 min), higher than that reported by other authors in the literature under the same conditions. In addition, $Pd_{bars}–SiO_2$ catalyst can be reused without significant loss of catalytic activity.

Acknowledgements

We gratefully acknowledge financial support from CICYT (MAT 2006-14274-C02-01) and Consolider-Ingenio-2010

(project MULTICAT). We would like to thank Dr. Juan García Rodriguez of the Universidad Complutense de Madrid for providing hydrogen chemisorption measurements and useful discussions.

References

[1] (a) J. March, Advanced Organic Chemistry: Reactions, Mechanisms and Structures, vol. 1, 3rd ed., 1993;
(b) T. Mallat, A. Baiker, Chem. Rev. 104 (2004) 3037–3058;
(c) G.F. Hutchings, Chem. Commun. (2008) 1148–1164.
[2] (a) A. Abad, P. Concepcion, A. Corma, H. Garcia, Angew. Chem. Int. Ed. 44 (2005) 4066–4069;
(b) A. Abad, C. Almela, A. Corma, H. Garcia, Chem. Commun. (2006) 3178–3180.
[3] (a) K. Mori, K. Yamaguchi, T. Hara, T. Mizugaki, K. Ebitani, K. Kaneda, J. Am. Chem. Soc. 124 (2002) 11572–11573;
(b) K. Mori, K. Yamaguchi, T. Hara, T. Mizugaki, K. Ebitani, K. Kaneda, J. Am. Chem. Soc. 126 (2004) 10657–10666.
[4] S.F.J. Hackett, R.M. Brydson, M.H. Gass, I. Harvey, A.D. Newman, K. Wilson, A.F. Lee, Angew. Chem. Int. Ed. 46 (2007) 8593–8596.
[5] (a) D.I. Enache, J.K. Edwards, P. Landon, B. Solsona-Espriu, A.F. Carley, A.A. Herzing, M. Watanabe, C.J. Kiely, D.W. Knight, G.J. Hutchings, Science 311 (2006) 362–365;
(b) P.J. Miedziak, Q. Heb, J.K. Edwardsa, S.H. Taylora, D.W. Knighta, B. Tarbitc, C.J. Kielyb, G.J. Hutchings, Catal. Today 164 (2011) 315–319.
[6] (a) N. Semagina, A. Renken, D. Laub, L. Kiwi-Minsker, J. Catal. 246 (2007) 308–314;
(b) N. Semagina, A. Renken, L. Kiwi-Minsker, J. Phys. Chem. C 111 (2007) 13933–13937.
[7] J. Chen, Q. Zhang, Y. Wang, H. Van, Adv. Synth. Catal. 350 (2008) 453–464.
[8] F. Li, Q. Zhang, Y. Wang, Appl. Catal. A: Gen. 334 (2008) 217–226.
[9] (a) R. Narayanan, M.A. El-Sayed, Nano Lett. 4 (2004) 1343;
(b) R. Narayanan, M.A. El-Sayed, J. Am. Chem. Soc. 126 (2004) 7194;
(c) N. Tian, Z.-Y. Zhou, S.-G. Sun, Y. Ding, Z.L. Wang, Science 316 (2007) 732.
[10] B.M. Choudary, R.S. Mulukutla, K.J. Klabunde, J. Am. Chem. Soc. 125 (2003) 2020–2021.
[11] K. Zhou, X. Wang, X. Sun, Q. Peng, Y. Li, J. Catal. 229 (2005) 206–212.
[12] R. Narayanan, M.A. El-Sayed, Langmuir 21 (2005) 2027–2033.
[13] (a) L. Piccolo, A. Valcarcel, M. Bausach, C. Thomazeau, D. Uzio, G. Berhault, Phys. Chem. Chem. Phys. 10 (2008) 5504–5506;
(b) C. Kim, H. Lee, Catal. Commun. 11 (2009) 7–10.
[14] (a) Y. Xiong, J. Chen, B. Wiley, Y. Xia, J. Am. Chem. Soc. 127 (2005) 7332–7333;
(b) Y. Xiong, J. Chen, B. Wiley, Y. Xia, Y. Yin, Z.-Y. Li, Nano Lett. 5 (2005) 1237–1242;
(c) Y. Xiong, J.M. McLellan, J. Chen, Y. Yin, Z.-Y. Li, Y. Xia, J. Am. Chem. Soc. 127 (2005) 17118–17127.
[15] (a) Y. Xiong, H. Cai, B.J. Wiley, J. Wang, M.J. Kim, Y. Xia, J. Am. Chem. Soc. 129 (2007) 3665–3675;
(b) Y. Xiong, J.M. McLellan, Y. Yin, Y. Xia, Angew. Chem. Int. Ed. 46 (2007) 790–794.
[16] Y. Sun, L. Zhang, H. Zhou, Y. Zhu, E. Sutter, Y. Ji, M.H. Rafailovich, J.C. Sokolov, Chem. Mater. 19 (2007) 2065–2070.
[17] Y. Piao, Y. Jang, M. Shokouhimehr, I.S. Lee, T. Hyeon, Small 3 (2007) 255–260.
[18] E. Reale, A. Leyva, A. Corma, C. Martinez, H. García, F. Rey, J. Mater. Chem. 15 (2005) 1742–1752.
[19] Y. Xiong, I. Washio, J. Chen, H. Cai, Z.-Y. Li, Y. Xia, Langmuir 22 (2006) 8563–8570.
[20] (a) S.A. Bagshaw, E. Prouzet, T.J. Pinnavaia, Science 269 (1995) 1242–1244;
(b) S. Hitz, R. Prins, J. Catal. 168 (1997) 194–206.
[21] B. Tian, X. Liu, C. Yu, F. Gao, Q. Luo, S. Xie, B. Tu, D. Zhao, Chem. Commun. (2002) 1186–1187.
[22] (a) R. Yu, H. Song, X.-F. Zhang, P. Yang, J. Phys. Chem. B 109 (2005) 6940–6943;
(b) R. Yu, H. Song, X.-F. Zhang, P. Yang, J. Phys. Chem. B 119 (2005) 1186–1187;
(c) S.H. Joo, J.Y. Park, C.-K. Tsung, Y. Yamada, P. Yang, G.A. Somorjai, Nat. Mater. 8 (2009) 126–131.
[23] (a) F. Baletto, R. Ferrando, Phys. Rev. B 63 (2001) 155408;
(b) F. Baletto, R. Ferrando, A. Fortunelli, F. Montalenti, C. Mottet, J. Chem. Phys. 116 (2002) 3856–3863.
[24] M.J. Kappers, J.T. Miller, D.C. Koningsberger, J. Phys. Chem. 100 (1996).
[25] (a) H. Borchert, B. Jürgens, V. Zielasek, G. Rupprechter, S. Giorgio, C.R. Henry, M. Bäumer, J. Catal. 247 (2007) 145–154;
(b) S. Bertarione, D. Scarano, A. Zecchina, V. Johánek, J. Hoffmann, S. Schauermann, M.M. Frank, J. Libuda, G. Rupprechter, H.J. Freund, J. Phys. Chem. B 108 (2004) 3603–3613;
(c) D. Ferri, C. Mondelli, F. Krumeich, A. Baiker, J. Phys. Chem. B 110 (2006) 22982–22986;
(d) T. Lear, R. Marshall, J.A. Lopez-Sanchez, S.D. Jackson, T.M. Klapötke, J. Chem. Phys. 123 (2005) 174706–174713.
[26] C.R. Henry, Surf. Sci. Rep. 31 (1998) 231–325.
[27] P. Concepcion, A. Corma, J. Silvestre-Albero, V. Franco, J.Y. Chane-Ching, J. Am. Chem. Soc. 126 (17) (2004) 5523.
[28] A. Abad, C. Almela, A. Corma, H. García, Tetrahedron 62 (2006) 6666–6672.
[29] T. Yasu-eda, R. Se-ike, N. -oki Ikenaga, T. Miyake, T. Suzuki, J. Mol. Catal. A: Chem. 306 (2009) 136–142.